

Allen Cell Types Database

TECHNICAL WHITE PAPER: BIOPHYSICAL MODELING – ALL ACTIVE

OVERVIEW

Single-cell characterization and model-development is key towards the creation of cell type taxonomies and their characterization. Specifically, with regards to computational model-development, a host of models of varying features and complexity are being developed. The ones described herein are biophysically realistic representations of neurons that include dendrites populated with active, Hodgkin Huxley-type nonlinear conductances.

Active dendritic conductances are one of the hallmarks of cortical neurons as they critically impact their input-output relationship: active dendritic conductances substantially impact synaptic integration properties along the neural morphologies as well as the somatic spiking response (Stuart *et al.*, 2007). As such, we describe an effort to create single-cell representations based on slice electrophysiology and morphology reconstruction data that capture such dendritic nonlinearities. To set up such biophysically realistic, single-neuron model optimizations, the Allen Institute collaborated with the Blue Brain Project (BBP, Switzerland, <http://bluebrain.epfl.ch>) to utilize their expertise in the development of such all-active single-cell biophysically realistic models (Druckmann *et al.*, 2007; Hay *et al.*, 2011), morphology analyses (Markram *et al.*, 2015) and usage of very large computational resources such as the Blue Gene Q (Reimann *et al.*, 2013; Markram *et al.*, 2015). The workflow for setting up and performing these optimizations is shown in **Figure 1**.

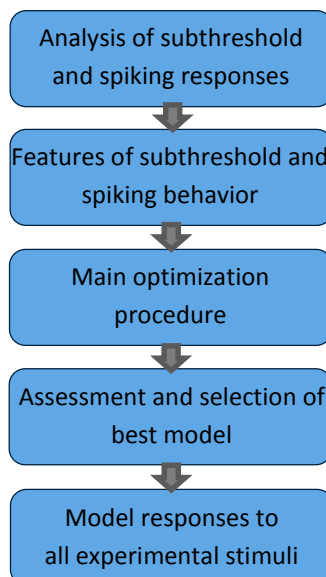


Figure 1. Summary of the generation of the all-active biophysically detailed single-neuron models.
Schematic illustration of the different steps involved in the generation of the single-neuron models.

FEATURE ANALYSIS

The optimization procedure of the single-neuron models is feature-based and attempts to populate the somatic, axonal, and dendritic properties in such manner as to capture features of intracellular somatic responses to a number of standardized current stimulation waveforms. Specifically, for each neuron experimentally whole-cell patched, biocytin-filled and morphologically reconstructed, a host of quality control criteria are applied to assess the quality of the electrophysiology recordings (See Electrophysiology Overview Technical White Paper in [Documentation](#)) as well as the morphological reconstruction (Morphology Overview Technical White Paper in [Documentation](#)). Given these criteria are met, the experiment is passed on for the analysis of subthreshold and spiking responses (**Figure 1**). Specifically, 11 electrophysiological features are extracted for each experiment and their mean and standard deviation (std) is computed for a particular stimulation waveform (**Table 1**). Notably, if equal or more than two repetitions of the same stimulation waveform exists (majority of the experiments), then the std of that particular waveform is used. If only a single repetition of the experiment existed, the default value of 5% is used for the std.

All features were extracted using the Electrophys Feature Extraction Library (eFEL) developed at the Blue Brain Project (<https://github.com/BlueBrain/eFEL>). For a list and description of all 11 features used for building the computational models see **Table 1** and **Figure 2**. The electrophysiology stimuli used for the feature extraction and optimization were: ShortDC, LongDC, Ramp, and LongDCSupra (see detailed description in the Electrophysiology Overview Technical White Paper in [Documentation](#)). For every feature, an absolute standard score was calculated $Z_i = \frac{|f_i - \mu_i|}{\sigma_i}$ with the feature value (f_i) measured from the output traces of the models, μ_i and σ_i the experimentally measured mean and standard deviation for the 11 features in the respective cells.

Table 1. Electrophysiology features used to constrain all-active, multi-compartmental models.

Feature Name	Description
mean_frequency	Mean frequency calculated as number of action potentials during stimulation divided by time between stimulus onset and last spike in Hz.
ISI_log_slope	Slope of loglog interspike intervals (ISI).
adaptation_index2	Normalized average difference of two consecutive ISI starting from second ISI.
time_to_first_spike	Time from stimulus onset to peak time of first spike in ms.
time_to_last_spike	Time from stimulus onset to peak time of last spike in ms.
AP_width	Mean of width at -20 mV of action potential (AP) in ms. Mean for all AP.
AP_height	Height at peak of action potential in mV. Mean for all AP.
min_voltage_between_spikes	Minimum voltage between two action potentials in mV. Mean for all ISI.
steady_state_voltage_stimend	The average voltage during the last 90% of the stimulus duration in mV.
voltage_base	The average voltage during the last 90% before stimulus onset in mV.
voltage_after_stim	The average voltage between 25% and 75% between end of stimulus and end of recording in mV.

MODEL CONFIGURATION

Morphology

Morphological reconstructions of neurons were analyzed using Blue Brain Project algorithms before placing into the workflow for optimization and model generation. Specifically, attention was paid to the relationship between dendritic diameter and the branch order. In general, the diameter of dendrites decreases with increasing distance from the soma resulting in a negative slope in the diameter-branch order relationship (Stuart *et al.*, 2007). The diameter-branch order relationship was analyzed for all morphologies and only those that showed an overall negative slope were accepted (*i.e.* overall decrease in dendritic diameter with increasing distance from the soma). Notably, some irregularities were observed along dendritic reconstructions with localized increases in diameter for farther away compartments. A limit of 15% was set on the (normalized) diameter increase per branch order: morphologies with local dendritic diameter increases larger than the limit were flagged and removed from the queue.

The compartments of excitatory neurons were separated into axon initial segment (AIS), soma, basal dendrites, and apical dendrites. For inhibitory neurons, there was only a single dendritic zone. The full axon was not simulated, but only the AIS. The AIS was represented by two fixed length sections with a total length of 60 μm and a diameter obtained from the reconstructed morphology.

Active and Passive Properties

In all models, passive and active properties were optimized in the same fitting procedure. For passive properties, one value for the specific capacitance (c_m), passive conductance (g_{pas}), passive reversal potential (e_{pas}), and cytoplasmic resistivity (R_a) was uniformly distributed across all compartments. Notably, the values of these parameters were part of the genetic optimization procedure. Active channel mechanisms were uniformly spatially distributed in the AIS, soma, and dendrites with every zone receiving a separate set of channels as shown in **Table 2**.

Apart from the spatial distribution, the ion channels were identical with those in the “perisomatic models” (see Neuronal Models: Biophysical-Perisomatic in [Documentation](#)). With the following exceptions, these channels were similar to those as described in Hay *et al.* (2011): The fast and persistent sodium currents have been replaced with an alternative kinetic model formulation from Carter *et al.* (2012) where the rate of inactivation depends allosterically on the extent of channel activation (NaV.mod). The slow inactivating potassium current has been replaced by two other potassium current models: one representing a Kv1-like current (Kd.mod) (Foust *et al.*, 2010) and another representing a Kv2-like current (Kv2like.mod) (Liu and Bean, 2014). Additionally, the original M-current has been replaced by a model from rat CA1 pyramidal neurons (Im_v2.mod) (Vervaeke *et al.*, 2006). This ion channel composition resulted in enhanced performance of the resulting models (as compared to the experimental data) with the specific equations and parameters described in the provided “.mod” files that define each mechanism for the NEURON simulation environment. All these active conductances were modeled using a Hodgkin-Huxley formulation.

The intracellular Ca^{2+} dynamics were modeled using a first-order ODE that simulated the entry of Ca^{2+} due to the transmembrane current into a 100 nm sub-membrane shell with buffering/pumping (CaDynamics.mod). In addition to c_m , e_{pas} , R_a , and the densities of active and passive ion channel conductances, also the time constant of Ca^{2+} removal (decay) and the ratio of free Ca^{2+} (γ) were included as free parameters in the optimization procedure. The complete list of free parameters and their minimum and maximum values as used in the optimization are shown in **Table 2**.

In total, the models were optimized with 26 free parameters: 18 active conductance densities, 4 intracellular Ca^{2+} dynamics parameters, and 4 passive parameters.

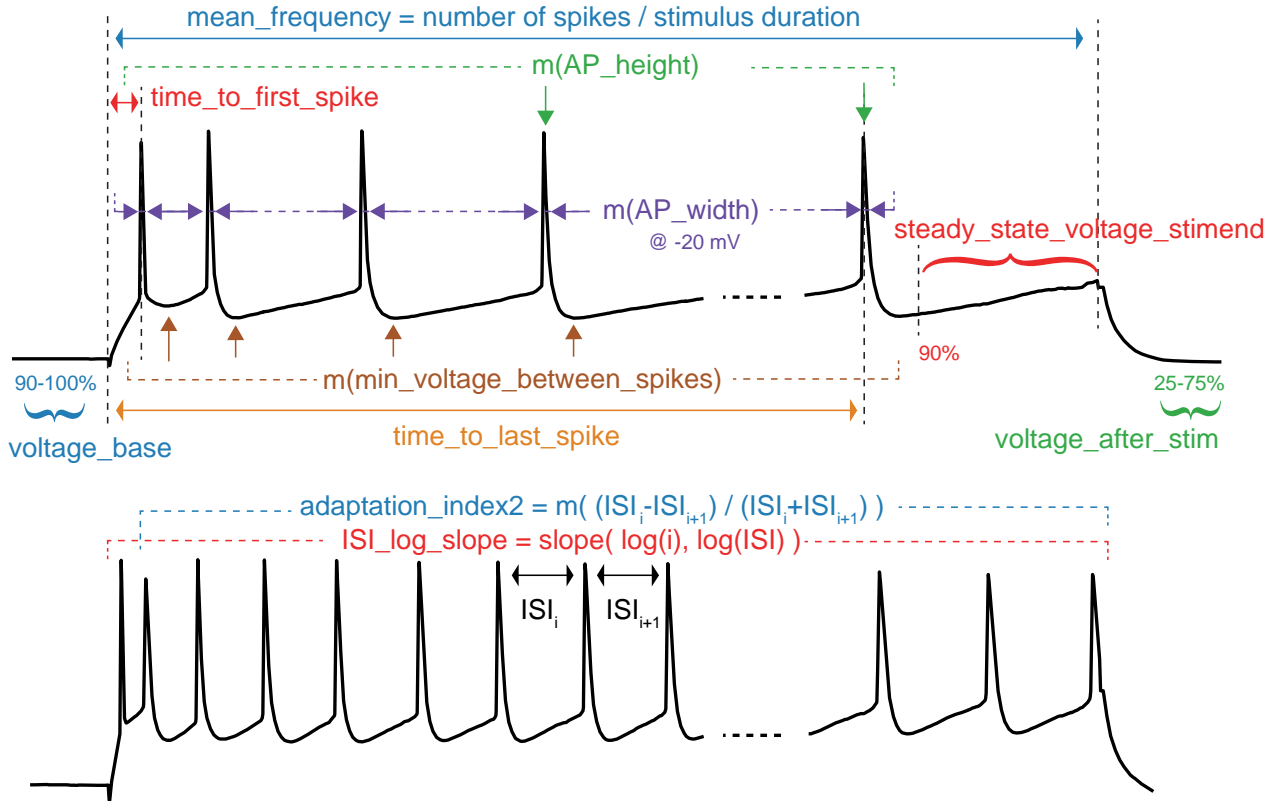


Figure 2. Illustration of all electrophysiological features.

Simulation Conditions

Simulations were performed in NEURON using the variable time step method. The equilibrium potentials of Na⁺ and K⁺ were set to values calculated from the internal and external solutions used in the *in vitro* experiments ($E_{Na} = +53 \text{ mV}$, $E_K = -107 \text{ mV}$). The equilibrium potential of Ca²⁺ was calculated during each time step by NEURON using the Nernst equation using $[Ca^{2+}]_o = 2 \text{ mM}$ and the value of $[Ca^{2+}]_i$ at that time (resting $[Ca^{2+}]_i$ was 100 nM). The temperature of the simulation also matched the temperature of the recording. All cells for which models were built were recorded at a temperature near 34°C (Electrophysiology Overview in [Documentation](#)). For active conductances based on data recorded at temperatures differing from these conditions, the kinetics were scaled with a Q10 of 2.3 (Hay *et al.*, 2011).

Table 2. Ionic conductances of excitatory neurons.

	AIS	Soma	Dendrites
Passive properties	cm (0.5 : 10 $\mu\text{F}/\text{cm}^2$)		
	g_pas (1e-7 : 1e-2 S/cm ²)		
	e_pas (-110 : -60 mV)		
	Ra (50 : 150 $\Omega\text{-cm}$)		
Sodium (NaV.mod)	gbar_NaV (1e-7 : 5e-2 S/cm ²)	gbar_NaV (1e-7 : 5e-2 S/cm ²)	gbar_NaV (1e-7 : 5e-2 S/cm ²)
Transient potassium (K_T.mod)	gbar_K_T (1e-7 : 1e-2 S/cm ²)		
Delayed rectifier (Kd.mod)	gbar_Kd (1e-7 : 1e-2 S/cm ²)		
Kv2-like potassium (Kv2like.mod)	gbar_Kv2like (1e-7 : 1e-1 S/cm ²)		
Kv3-like potassium (Kv3_1.mod)	gbar_Kv3_1 (1e-7 : 1 S/cm ²)	gbar_Kv3_1 (1e-7 : 1 S/cm ²)	gbar_Kv3_1 (1e-7 : 1 S/cm ²)
SK-type potassium (SK.mod)	gbar_SK (1e-7 : 1e-2 S/cm ²)	gbar_SK (1e-7 : 1e-2 S/cm ²)	
Low-voltage activated calcium (Ca_LVA.mod)	gbar_Ca_LVA (1e-7 : 1e-2 S/cm ²)	gbar_Ca_LVA (1e-7 : 1e-2 S/cm ²)	
High-voltage activated calcium (Ca_HVA.mod)	gbar_Ca_HVA (1e-7 : 1e-4 S/cm ²)	gbar_Ca_HVA (1e-7 : 1e-4 S/cm ²)	
Calcium dynamics (CaDynamics.mod)	gamma_CaDynamics (5e-4 : 5e-2 %)	gamma_CaDynamics (5e-4 : 5e-2 %)	
	decay_CaDynamics (20 : 1000 ms)	decay_CaDynamics (20 : 1000 ms)	
Hyperpolarization-activated (Ih.mod)		gbar_Ih (1e-7 : 1e-5 S/cm ²)	gbar_Ih (1e-7 : 1e-5 S/cm ²)
M-like potassium (Im_v2.mod)			gbar_Im_v2 (1e-7 : 1e-2 S/cm ²)

OPTIMIZATION PROCEDURE

Genetic Algorithm

For the optimization, the C++ optimiser framework from the Blue Brain Project was used (Markram *et al.*, 2015). This framework integrates the NEURON simulation environment, the indicator-based evolutionary algorithm (IBEA) from the optimisation library PISA (Bleuler *et al.*, 2003), and the feature extraction library eFEL. For each model the evolutionary algorithm was run twice with two different initial random seeds each with a population size of typically 1024 individuals on 512 cores of a BlueGene/P system for 100 generations. After the optimization, the two best individuals with the smallest sum of their objective values for each seed were selected to be tested in the model generalization procedure. Taking into account the generalization results, the best solution among these four models was selected and became the final electrical model (**Figure 3**).

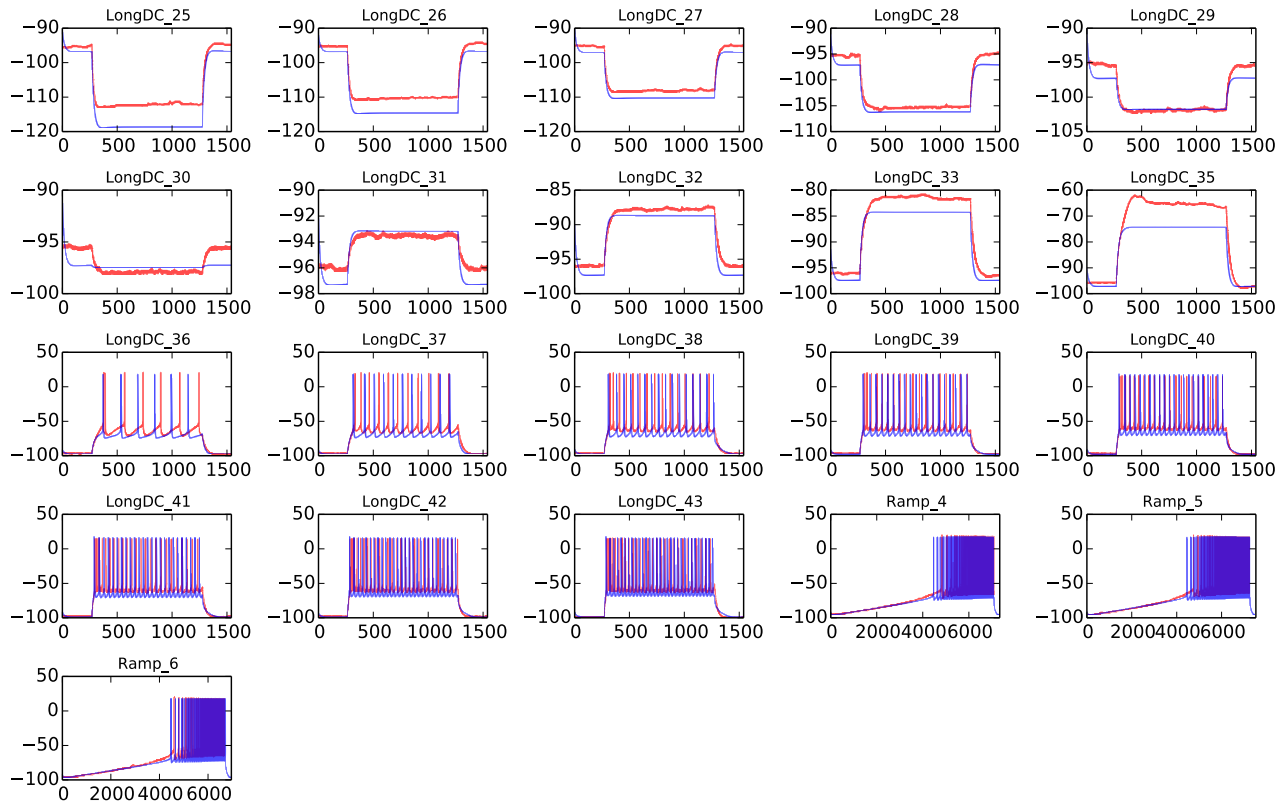


Figure 3. Illustration of experimental and model traces.

The somatic intracellular voltage traces for various stimulation protocols for an experiment (red) and the associated all-active biophysically realistic model (blue) developed via the optimization framework.

Model Evaluation

Once the best model was selected, all stimulation protocols from the experiment were replayed – importantly, these not only included the stimulation waveforms used to produce the model (ShortDC, LongDC, LongSupra, and Ramp) but various “noise” input waveforms. Response of the model to the latter ones was used to evaluate the model in terms of various metrics such as explained variance and waveform similarity (**Figure 4**).

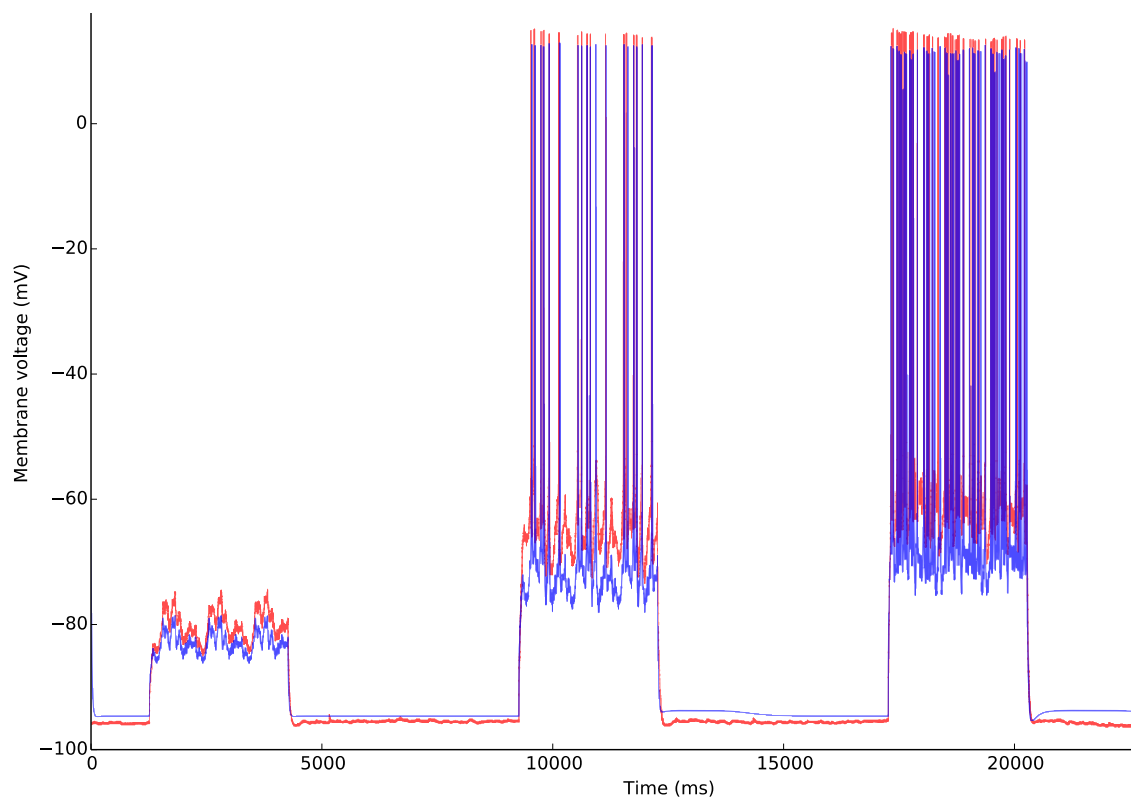


Figure 4. Noise stimulation is used to evaluate the model.

Noise stimulation waveforms are administered as part of the model evaluation step (red: experiment; blue: simulation). One of the measures used to assess the quality of the model is the explained variance metric. For the illustrated experiment, the explained variance is 0.84.

MODEL GENERALIZATION

Limitations of the Model

While dendritic nonlinearities were accounted for in our optimizations and model generation, it has to be remarked that the actual experimental data considered were somatic intracellular responses to stereotyped current injections. Given this experimental setup, information about exact dendritic events and processes remains limited as the dominating events under these conditions are due to somatic electrogenesis. This is particularly true for dendritic events occurring many hundreds of micrometers away from the soma. In our optimizations the spatially constant distribution of Ih channels (hyperpolarization-activated cation current) reported for layer 5 pyramidal neurons in mouse V1 was taken into account (Shai *et al.*, 2015). Yet, it remains unclear whether such constant spatial scaling applies for the other nonlinear dendritic conductances. Finally, in this version of the all-active product the apical Ca hotzone located close to the main apical bifurcation known to elicit dendritic Ca²⁺-spikes was not taken into account (Shai *et al.*, 2015).

REFERENCES

Bleuler S, Laumanns M, Thiele L, and Zitzler E (2003) PISA—A Platform and Programming Language Independent Interface for Search Algorithms. In CM Fonseca *et al.*, editors, *Conference on Evolutionary Multi-Criterion Optimization (EMO 2003)*, volume 2632 of LNCS, pp. 494–508, Berlin, Springer.

Carter BC, Giessel AJ, Sabatini BL, Bean BP (2012) Transient sodium current at subthreshold voltages: activation by EPSP waveforms. *Neuron* 75:1081–1093.

Druckmann S, Banitt Y, Gidon A, Schuermann F, Markram H, Segev I (2007) A novel multiple objective optimization framework for constraining conductance-based neuron models by experimental data. *Frontiers in Neuroscience* 1:7-18.

Foust AJ, Yu Y, Popovic M, Zecevic D, McCormick DA (2011) Somatic membrane potential and Kv1 channels control spike repolarization in cortical axon collaterals and presynaptic boutons. *Journal of Neuroscience* 31:15490-15498.

Hay E, Hill S, Schürmann F, Markram H, Segev I (2011) Models of neocortical layer 5b pyramidal cells capturing a wide range of dendritic and perisomatic active properties. *PLoS Computational Biology* 7:e1002107.

Liu PW, Bean BP (2014) Kv2 channel regulation of action potential repolarization and firing patterns in superior cervical ganglion neurons and hippocampal CA1 pyramidal neurons. *Journal of Neuroscience* 34:4991-5002.

Markram H, Muller E, Ramaswamy S, Reimann MW, Abdellah M, Sanchez CA, Ailamaki A, Alonso-Nanclares L, Antille N, Arsever S, Kahou GA, Berger TK, Bilgili A, Buncic N, Chalimourda A, Chindemi G, Courcol JD, Delalondre F, Delattre V, Druckmann S, Dumusc R, Dynes J, Eilemann S, Gal E, Gevaert ME, Ghobril JP, Gidon A, Graham JW, Gupta A, Haenel V, Hay E, Heinis T, Hernando JB, Hines M, Kanari L, Keller D, Kenyon J, Khazen G, Kim Y, King JG, Kisvarday Z, Kumbhar P, Lasserre S, Le Bé JV, Magalhães BR, Merchán-Pérez A, Meystre J, Morrice BR, Muller J, Muñoz-Céspedes A, Muralidhar S, Muthurasa K, Nachbaur D, Newton TH, Nolte M, Ovcharenko A, Palacios J, Pastor L, Perin R, Ranjan R, Riachi I, Rodríguez JR, Riquelme JL, Rössert C, Sfyarakis K, Shi Y, Shillcock JC, Silberberg G, Silva R, Tauheed F, Telefont M, Toledo-Rodríguez M, Tränkler T, Van Geit W, Díaz JV, Walker R, Wang Y, Zaninetta SM, DeFelipe J, Hill SL, Segev I, Schürmann F (2015) Reconstruction and Simulation of Neocortical Microcircuitry. *Cell* 163:456-492.

Reimann MW, Anastassiou C, Perin R, Hill SL, Markram H, Koch C (2013) A biophysically detailed model of neocortical local field potentials predicts the critical role of active membrane currents. *Neuron* 79: 375-390.

Shai AS, Anastassiou CA, Larkum ME, Koch C (2015) Physiology of layer 5 pyramidal neurons in mouse primary visual cortex: coincidence detection through bursting. *PLoS Computational Biology* 11:e1004090.

Stuart G, Spruston N, Häusser M (2007) *Dendrites*. Oxford University Press, New York.

Vervaeke K, Hu H, Graham LJ, Storm JF (2006) Contrasting effects of the persistent Na⁺ current on neuronal excitability and spike timing. *Neuron* 49:257-270.